# THE FENDER BASSMAN 5F6-A FAMILY OF PREAMPLIFIER CIRCUITS—A WAVE DIGITAL FILTER CASE STUDY

*W. Ross Dunkel*[*], *Maximilian Rest* [†*], *Kurt James Werner*[*], *Michael Jørgen Olsen*[*], *Julius O. Smith III*[*]

[*]Center for Computer Research in Music and Acoustics (CCRMA), Stanford University, California, USA
[†]Fakultät Elektrotechnik und Informatik, Technische Universität Berlin, Berlin, Germany
[chigi22|mrest|kwerner|mjolsen|jos]@ccrma.stanford.edu

## ABSTRACT

The Fender Bassman model 5F6-A was released in 1958 and has become one of the most revered guitar amplifiers of all time. It is the progenitor of a long line of related Fender designs in addition to inspiring Marshall's first amplifier design. This paper presents a Wave Digital Filter study of the preamplifier circuit of 5F6-A-based amplifiers, utilizing recent theoretical advances to enable the simultaneous simulation of its four nonlinear vacuum tube triodes. The Dempwolf triode model is applied along with an iterative Newton solver to calculate the scattering at the 25 port R-type adapter at the root of the WDF tree. Simulation results are compared to "ground truth" SPICE data showing excellent agreement.

## 1. INTRODUCTION

The Fender Bassman amplifier was first introduced in 1952, undergoing multiple revisions before culminating in the seminal 5F6-A version in 1958. This model is one of the most revered and imitated amplifier circuits of all time [1], inspiring countless related designs including the first Marshall—the JTM 45. Introduced in 1962 by London music store owner Jim Marshall, the JTM 45's original design borrowed heavily from the 5F6-A, a popular seller and employee favorite [2]. The JTM 45 quickly became a successful and much-praised amplifier in its own right and was a crucial ingredient in the heady brew of hard rock, blues, and psychedelic music that was the sound of 1960s London. Our goal is to develop efficient, re-configurable digital emulations of the 5F6-A, JTM 45 and related circuits to serve as a research and design tool for DIY amp-designers, circuit benders, and sonic historians considering the evolution of this historic circuit.

A number of different approaches have been taken to the numerical simulation of vacuum tube guitar amplifier circuits over the years. For an historical overview as well as an introduction to the physical principles of operation of triode tubes see [3]. Recent years have seen the increased use of Wave Digital Filters (WDFs) [4] as an effective tool for virtual analog modeling of audio circuits [5]. New theoretical advances have enabled WDFs to model circuits with complex topologies [6] and multiple nonlinearities [7], a category that includes many audio circuits of interest. In this paper we apply these techniques to the construction of a WDF model of Bassman 5F6-A-derived preamplifiers. These circuits provide an ideal case study—they contain multiple vacuum tube triodes in a complex circuit topology but with a modest part count, limiting overall system complexity to a reasonable level.

The remainder of this work is structured as follows: Sec. 2 explores the circuit in detail, Sec. 3 reviews necessary background information and derives the structure of the WDF simulation including the novel application of the Dempwolf triode model and a Newton-based root finder, Sec. 4 presents simulation results, and Sec. 5 summarizes future work and conclusions.

## 2. BASSMAN 5F6-A PREAMPLIFIER CIRCUITS

This work defines the 5F6-A's "preamplifier circuit" as consisting of the following stages: the 12AY7 preamp, 12AX7 voltage amp, and 12AX7 cathode follower (as in [1]) driving a nominal load resistance $R_L$. The circuit schematic is shown in Figure 1 with component values listed in Table 1. The tone stack is not included in the simulation as it is buffered from the preceding sections by the cathode follower stage. The tone stack has already been considered in the context of WDFs [8, 9] and in an earlier non-WDF study [10]. Nominal values cited in the remainder of Sec. 2 are taken from [1] and are presented solely to provide insight into the circuit's operation.

| Edge | Comp | Value | Edge | Comp | Value |
|---|---|---|---|---|---|
| 1 | $R_{GB1A}$ | 68 kΩ | 14 | $R_{VBP}$ | $\alpha R_{\text{vol}}$ |
| 2 | $R_{GB1B}$ | 68 kΩ | 15 | $R_{VBN}$ | $(1-\alpha)R_{\text{vol}}$ |
| 3 | $R_{IB}$ | 1 MΩ | 16 | $R_{VNN}$ | $(1-\alpha)R_{\text{vol}}$ |
| 4 | $R_{K1}$ | 1 MΩ | 17 | $R_{VNP}$ | $\alpha R_{\text{vol}}$ |
| 5 | $C_{K1}$ | 250 µF | 18 | $C_{B1}$ | 100 pF |
| 6 | $R_{GN1A}$ | 68 kΩ | 19 | $R_{GB2}$ | 270 kΩ |
| 7 | $R_{GN1B}$ | 68 kΩ | 20 | $R_{GN2}$ | 270 kΩ |
| 8 | $V_{\text{in}}$ | – | 21 | $R_{P2}$ | 100 kΩ |
| 9 | $R_{IN}$ | 1 MΩ | 22 | $R_{K2}$ | 820 Ω |
| 10 | $R_{PB}$ | 100 kΩ | 23 | $R_L$ | 100 kΩ |
| 11 | $R_{PN}$ | 100 kΩ | 24 | $V_P$ | 310 V |
| 12 | $C_{ON}$ | 20 nF | 25 | $C_{B2}$ | 556 pF |
| 13 | $C_{OB}$ | 20 nF | – | $R_{\text{vol}}$ | 1 MΩ |

Table 1: *Circuit Components*

### 2.1. The Preamp Section

The preamp's first stage is a dual channel inverting amplifier powered by a 12AY7 tube consisting of triodes $T_{1B}$ and $T_{1N}$ for bright and normal channels respectively. The grid stopper resistors $R_{GB1A}$, $R_{GB1B}$, $R_{GN1A}$, $R_{GN1B}$ combine with the triodes' Miller capacitances [11] to form a low-pass filter that suppresses RF interference. Each channel has two inputs: high sensitivity #1 with input resistances $R_{IB}$ and $R_{IN}$ and voltage gain of $-32.2$ and low sensitivity #2 with input resistances of $R_{GB1A} + R_{GB1B}$ and $R_{GN1A} + R_{GN1B}$ and voltage gain of $-16.1$ (−6 dB attenuation relative to #1). With no cables inserted in the input jacks, their tip and switch terminals are shorted as shown on the left-hand side of Figure 1. When a cable is inserted, this connection is broken and

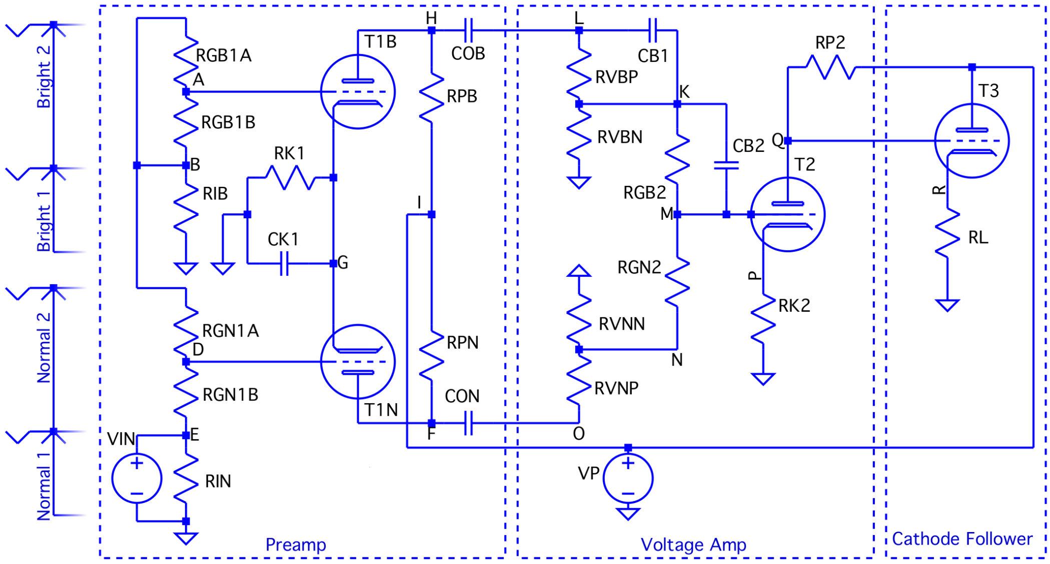


Figure 1: *5F6-A/JTM 45 preamplifier circuit with no inputs (left) and using Normal 1 input with a jumper between Normal 2 and Bright 1 (right). Circuit element values are listed in Table 1.*

the tip terminal is routed into the larger circuit as shown on the right. The cathode resistor $R_K$ sets the bias point of the triodes and is fully bypassed by the capacitor $C_K$ at audio frequencies. The output voltage of this section is developed across plate resistors $R_{PB1}$ and $R_{PB2}$ and is transmitted to the next stage through the output coupling capacitors $C_{OB}$ and $C_{ON}$.

### 2.2. The Voltage Amp Section

The second stage consists of a 12AX7 triode $T_2$ in an inverting amplifier configuration with a net voltage gain of $-20.7$ at maximum volume. Bright and normal volume levels are set via $1\,\mathrm{M}\Omega$ potentiometers parameterized by $\alpha_B$ and $\alpha_N$ respectively with $0 \leq \alpha \leq 1$, sub-dividing the pots into resistors $R_{VBN} = (1-\alpha)\cdot R_{\text{vol}}$, $R_{VBP} = \alpha \cdot R_{\text{vol}}$, $R_{VNN} = (1-\alpha)\cdot R_{\text{vol}}$, and $R_{VNP} = \alpha \cdot R_{\text{vol}}$. In practice these resistors are restricted to $R \geq 1\,\Omega$ and we consider only the case $\alpha_B = \alpha_N = \alpha$. Capacitors $C_{B1}$ and $C_{B2}$ provide the treble boost that gives the bright channel its name and $R_{GB1}$ and $R_{GB2}$ are again grid stopper resistors. Cathode resistor $R_{K2}$ sets $T_2$'s bias, with average plate current on the order of 1 mA. As will be seen in the results section, this triode's grid current can grow to an appreciable fraction of the overall cathode current at higher volume settings.

### 2.3. The Cathode Follower Section

The third section employs a 12AX7 triode $T_3$ in a non-inverting cathode follower configuration with slightly below unity gain ($\approx 0.984$). This stage presents a low output impedance of $615\,\Omega$, effectively decoupling it from the tone stack and making it an ideal final stage in our WDF simulation. Even more dramatically than in the case of $T_2$, $T_3$'s grid current can become appreciable at higher volumes. This has a significant impact on the preamplifier's output waveform, leading to asymmetric clipping and its concomitant even order harmonics. For this reason, models that fail to take grid current into account are unable to satisfactorily reproduce the sound of an over-driven guitar preamplifier.

### 2.4. Marshall JTM 45

The pre-amp of the JTM 45 is nearly identical to the 5F6-A with three important exceptions. First, a higher gain ECC83 (12AX7) replaces the Bassman's 12AY7 triodes $T_{1B}$ and $T_{1N}$ in the preamp section producing more overall gain and slightly different loading characteristics. Second, the lead version of the JTM 45 includes an additional bypass capacitor $C_{B2}$ across the bright input to $T_2$ that is not present in the 5F6-A, leading to a more pronounced treble boost for the bright channel. Third, the plate supply voltage $V_P$ is reduced from 325 V to 310 V [1]. For reasons discussed in Sec. 3.4, this work will specifically consider the JTM 45 preamplifier.

### 2.5. Jumpers

It is common for guitar players to explore different tones by employing a jumper cable between two of the unused input channels. This practice can appreciably alter the amplifier's overall response and further complicate the circuit's already complex topology. This case study specifically considers only one of the most common configurations [12] using the Normal #1 input with a jumper between Normal #2 and Bright #1 inputs as shown in Figure 1. A more general model incorporating real-time switchable jumpers will be the subject of future work.

## 3. WDF CIRCUIT SIMULATION

### 3.1. Previous Work

Wave Digital Filters (WDFs) are efficient, modular filter structures with attractive numerical properties including low sensitivity to coefficient round-off and guaranteed incremental passivity of passive circuit elements (capacitors, inductors, resistors, etc.) when simple rounding rules are applied [4]. Using other numerical methods these "passive" elements can become locally active with rounding error pumping energy into the system if care is not taken to ensure energy conservation. WDFs were invented to facilitate the design of digital emulations of analog ladder and lattice filters, which not coincidentally also feature low sensitivity to component value variance. Recent years have seen steady growth in the application of WDFs to other areas of study removed from their original intended use, including virtual analog modeling of audio circuits [5].

Early WDF tube amplifier studies [13] often modeled triodes as one port devices, ignoring grid current completely and using grid voltage as a cross-control on the plate port current. The classic Fairchild 670 compressor was modeled [14] using a similar approach with additional unit delays to decouple the push/pull amplifier sections. An enhanced model [15] more accurately captured triode behavior, modeling the plate-to-cathode port via a nonlinear resistor parametrized by Koren's model [16] and grid current via a diode model. However, this approach still relies on unit delays to yield computable structures. A case study by Pakarinen et al. [17] applies this model to the output chain of a vacuum tube amplifier. An iterative secant-method based solver has also been employed [18] to simultaneously solve the coupled equations of the Cardarilli triode model [19].

Two recent theoretical developments have enabled the use of WDFs to model vacuum tube circuits without making any of the ad-hoc assumptions of earlier work. First, an approach informed by Modified Nodal Analysis (MNA) [20] was developed to model complex circuit topologies that cannot be decomposed into simple series and parallel combinations [6]. Second, the use of this approach was extended to circuits containing multiple non-adaptable nonlinear ports [7]. Crucially these new developments separate nonlinearities from topology, ensuring that the most challenging part of the problem (solving for the scattering at the root) scales with the number of nonlinear ports instead of the total system size.

### 3.2. WDF Simulation Structure

Following the methodology of [6] the first step is to translate the schematic into the biconnected graph shown in Figure 2 with nodes representing physical circuit nodes and edges representing circuit components. The three unlabeled nodes in Figure 2 have been added to group the nonlinearities into a nonseparable replacement graph. The separation methods described in [21] can then be applied to reduce the graph into the set of split components show in Figure 3. These split components are used to construct the SPQR-tree representation shown in Figure 4 with the $\mathcal{R}$-type node at the root of the tree, connected via real edges to the $\mathcal{Q}$-type nodes and virtual edges to the $\mathcal{S}$-type and $\mathcal{P}$-type nodes.

This representation directly yields the WDF structure shown in Figure 5 with the $\mathcal{R}$-type node at the root and 17 child sub-trees. The problem then becomes solving for the scattering of incoming waves $\boldsymbol{a}$ to outgoing waves $\boldsymbol{b}$ at the root $\mathcal{R}$-type node governed by the equation

$$\boldsymbol{b} = \mathbf{S}\boldsymbol{a}\,. \tag{1}$$

The topological scattering matrix $\mathbf{S}$ can be calculated [6] using

$$\mathbf{S} = \mathbf{I} + 2\begin{bmatrix}\mathbf{0} & \mathbf{R}\end{bmatrix}\mathbf{X}^{-1}\begin{bmatrix}\mathbf{0} & \mathbf{I}\end{bmatrix}^{\mathsf{T}}\,, \tag{2}$$

where $\mathbf{R}$ is the diagonal matrix of port resistances and $\mathbf{X}$ is the MNA matrix. Omitted here due to space constraints, a full derivation of $\mathbf{X}$ for the JTM 45 can be found in the supplemental materials online [22]. Note that the nonlinearities have been absorbed into the $\mathcal{R}$-type node and are considered to be connected to the topological scattering via "internal ports" while "external ports" connect the root element to its sub-trees. Internal incoming and outgoing wave variables are denoted as $\boldsymbol{a}_I$ and $\boldsymbol{b}_I$ respectively, external waves as $\boldsymbol{a}_E$ and $\boldsymbol{b}_E$. We can then decompose equation (1) in terms of the vector nonlinear function $\boldsymbol{a}_I = f(\boldsymbol{b}_I)$ that maps $\boldsymbol{a}_I$ to $\boldsymbol{b}_I$ and the partitioned $\mathbf{S}$-matrix as

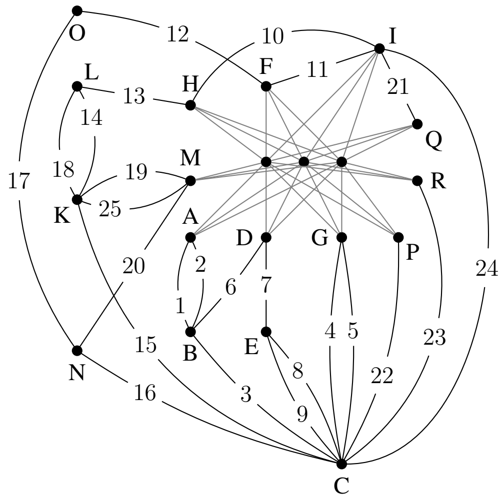


Figure 2: *Biconnected circuit graph. Node labels correspond to those in figure 1, edge numbers are defined in table 1.*

$$\text{wave nonlinearity} \quad \left\{\boldsymbol{a}_I = f(\boldsymbol{b}_I)\right. \tag{3}$$

$$\text{scattering} \quad \begin{cases}\boldsymbol{b}_I = \mathbf{S}_{11}\boldsymbol{a}_I + \mathbf{S}_{12}\boldsymbol{a}_E & (4)\\ \boldsymbol{b}_E = \mathbf{S}_{21}\boldsymbol{a}_I + \mathbf{S}_{22}\boldsymbol{a}_E\,. & (5)\end{cases}$$

These equations comprise a non-computable, delay-free loop as the outgoing internal wave variables depend instantaneously on the incoming waves that in turn depend instantaneously on $\boldsymbol{b}_I$.

The vast majority of nonlinear circuit elements lack a closed-form wave domain description and are therefore most commonly and straightforwardly defined in the Kirchhoff domain. We denote the vector Kirchhoff nonlinear function that maps voltage into current as $h(\boldsymbol{v}_C)$. In the case of the 5F6-A preamplifier this function is eight dimensional, consisting of four identical two-port triode models of two equations each (discussed in 3.4). When utilizing a Kirchhoff nonlinearity a wave-to-Kirchhoff conversion matrix $\mathbf{C}$ must be included and is partitioned into internal and external components as with the scattering matrix $\mathbf{S}$. These further definitions yield the following set of equations:

$$\begin{cases}\boldsymbol{i}_C = h(\boldsymbol{v}_C)\\ \boldsymbol{v}_C = \mathbf{E}\boldsymbol{a}_E + \mathbf{F}\boldsymbol{i}_C\\ \boldsymbol{b}_E = \mathbf{M}\boldsymbol{a}_E + \mathbf{N}\boldsymbol{i}_C\end{cases} \quad \text{with} \quad \begin{aligned}\mathbf{H} &= (\mathbf{I} - \mathbf{C}_{22}\mathbf{S}_{11})^{-1}\\ \mathbf{E} &= \mathbf{C}_{12}(\mathbf{I} + \mathbf{S}_{11}\mathbf{H}\mathbf{C}_{22})\mathbf{S}_{12}\\ \mathbf{F} &= \mathbf{C}_{12}\mathbf{S}_{11}\mathbf{H}\mathbf{C}_{21} + \mathbf{C}_{11}\\ \mathbf{M} &= \mathbf{S}_{21}\mathbf{H}\mathbf{C}_{22}\mathbf{S}_{12} + \mathbf{S}_{22}\\ \mathbf{N} &= \mathbf{S}_{21}\mathbf{H}\mathbf{C}_{21}\,.\end{aligned} \tag{6}$$

By setting up the problem in this way, the delay-free loop has been confined to a set of equations whose size equals the number

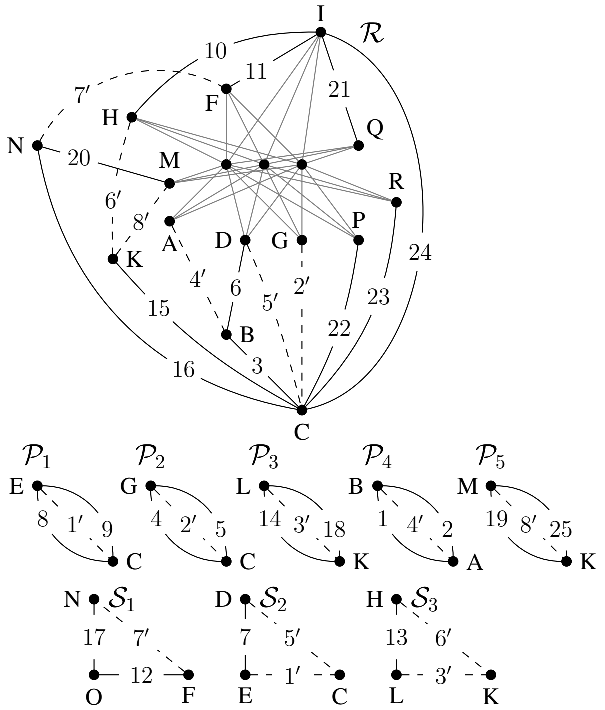


Figure 3: *$\mathcal{S}$-, $\mathcal{P}$-, and $\mathcal{R}$-type split components of the biconnected circuit graph.*

of nonlinear ports. Werner et al. chose to resolve the delay-free loop by applying the K-method to shear the nonlinearity [6]. As the sheared nonlinearity has no closed-form solution, its values are tabulated and interpolated at run-time. This approach has the drawback that as the number of nonlinear ports in the circuit grows a compromise between table resolution and an increasingly rapidly ballooning memory footprint must be made.

### 3.3. Newton's Method with Backtracking

For this study we take a different approach, directly applying a Newton solver to the set of nonlinear equations (6), eliminating the need to store and interpolate tables. Newton solvers have the further benefit of giving the algorithm designer access to the tradeoff space between accuracy and computation time via a single tunable

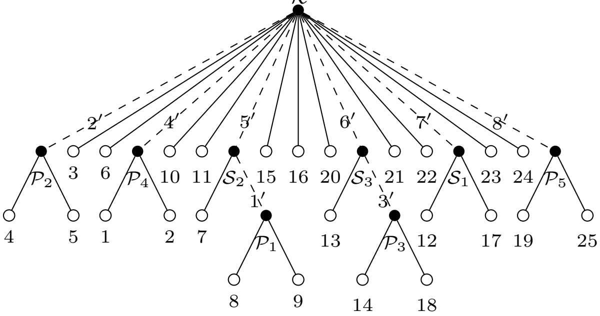


Figure 4: *SPQR tree representation of the circuit graph.*

tolerance parameter. The relevant entries of (6) can be re-arranged to make it clear that the problem can be stated in terms of finding the roots of the eight-dimensional equation

$$f\left(\boldsymbol{v}_C\right) = \mathbf{E}\boldsymbol{a}_E - \boldsymbol{v}_C + \mathbf{F}h\left(\boldsymbol{v}_C\right). \tag{7}$$

Specifically a form of Newton's method is used that includes backtracking to improve convergence robustness for a wide range of operating conditions. Initial guesses for the port voltages at the beginning of each audio sample's Newton iterations are calculated using the current value of the incoming external waves and the previous value of the internal port currents according to

$$\boldsymbol{v}_{C0}[n] = \mathbf{F}\boldsymbol{i}_C[n-1] - \mathbf{E}\boldsymbol{a}_E[n]. \tag{8}$$

A more detailed discussion of the use of Newton's method with backtracking in the context of WDFs is presented in [23]. Again, it is emphasized that the dimensionality of the iterative Newton root-finding in the current work is limited to the number of nonlinear ports.

### 3.4. Triode Model

The final step required to arrive at a working WDF simulation is to define an appropriate triode model. We consider the three-terminal electrical device as a two-port nonlinear WDF element with port voltages $V_{PK}$ and $V_{GK}$ and corresponding port currents $I_{PK}$ and $I_{GK}$. We adopt the convention of amplifier texts such as [1] with the letter "P" referring to plate, "G" to grid and "K" to cathode. Further, we use a two-letter naming convention to make explicit that all voltages are referenced to the cathode voltage. See Figure 6) for a graphical representation of these port definitions.

Previous WDF triode circuit studies have employed the Cardarilli model [19] which defines grid and plate currents in a piece-wise manner above and below a critical grid voltage $V_{GK} = 0.2\,\mathrm{V}$ as shown in Figure 7. The piece-wise nature of the model can lead to poor performance with Newton-based root finders near this critical voltage. Therefore this study employs the Dempwolf model [24] which features a smooth transition across the critical voltage. Cathode, grid, and plate currents are defined as follows:

$$\begin{aligned} I_K &= G \cdot \left( \log\left(1 + \exp\left(C \cdot \left(\frac{1}{\mu} \cdot V_{PK} + V_{GK}\right)\right)\right) \cdot \frac{1}{C} \right)^{\gamma} \\ I_{GK} &= G \cdot \left( \log\left(1 + \exp\left(C_g \cdot V_{GK}\right)\right) \cdot \frac{1}{C_g} \right)^{\xi} \\ I_{PK} &= I_K - I_{GK}. \end{aligned} \tag{9}$$

The model parameters are perveances $G$, $G_\mathrm{g}$, adaption parameters $C$, $C_\mathrm{g}$ and (positive) exponents $\gamma$, and $\xi$. For a discussion of the physical interpretation of these parameters and how to extract them from measured triode data see [24]. As the paper presents only 12AX7 triode parameters we choose to begin our investigation of the Bassman family of preamplifiers with the JTM 45. Evaluation of the perceptual accuracy of the Dempwolf model in the current work will be limited as it is impossible without physical measurements with which to compare. A comparison of various triode models to measurements of a physical amplifier will be the subject of future work.

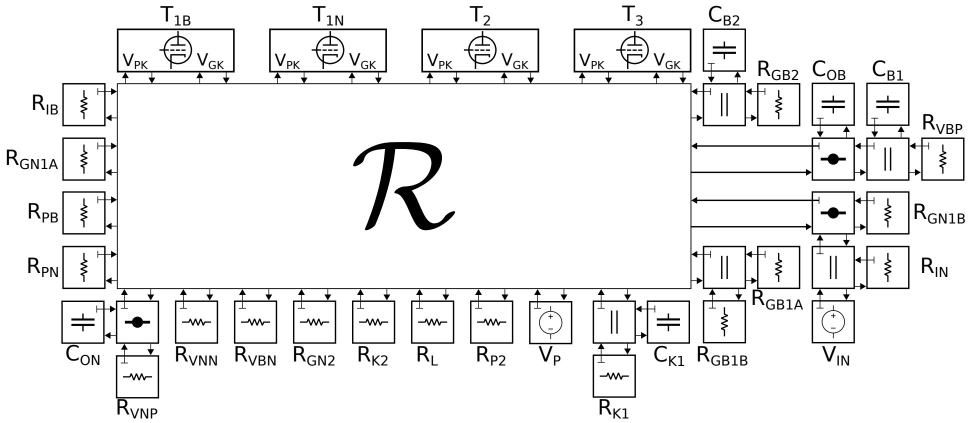


Figure 5: *Preamplifier WDF structure. The root of the tree is the large $\mathcal{R}$-type node, represented here as a topological scattering matrix connected to the four nonlinear triodes via eight "internal ports" and to seventeen linear, adapted sub-trees via its "external ports."*

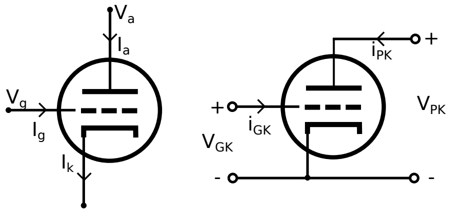


Figure 6: *Dempwolf triode current and voltage definitions (left) and port variable definitions (right).*

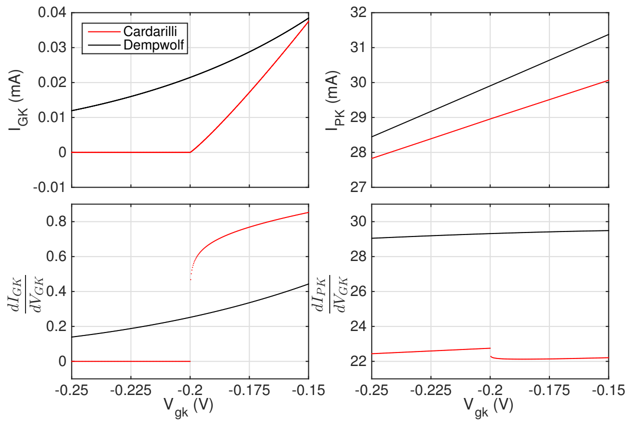


Figure 7: *Comparison of Cardarilli and Dempwolf grid ($I_{GK}$, left) and plate ($I_{PK}$, right) currents (above) and their derivatives (below) with respect to $V_{GK}$ for fixed plate voltage $V_{PK}$ = 150 V.*

## 4. RESULTS

For rendered example audio output see the supplemental materials online [22]. All simulation results presented here were performed in MATLAB at $4\times$ oversampling of a typical base audio sampling rate of 44.1 kHz (176.4 kHz) using 1 kHz, 125 mV peak-to-peak sinusoids as input signals unless otherwise noted. This voltage was chosen as a middle ground between the output level of a hot single coil and a lower-output humbucker pickup [25]. WDF results are compared to LTspice simulations carried out with an identically parameterized Dempwolf triode model. Time domain results for $\alpha$ values of 0.25, 0.5, 0.75, and 1.0 are presented in Figure 8, showing excellent agreement with SPICE results for all volume settings. For $\alpha = 0.25$, the output waveform is still highly sinusoidal but as volume is raised to $\alpha = 1.0$ soft clipping distortion characteristic of tube-based amplifiers becomes increasingly apparent. As $\alpha$ raised further the soft-clipping of the output waveform becomes increasingly asymmetric with positive excursions being noticeably flatter than negative excursions.

Figure 9 provides a more detailed view of the time domain simulation results for $\alpha = 1.0$, showing the output voltage waveform, currents $I_{PK}$ and $I_{GK}$ for triodes $T_2$ and $T_3$, error signal (defined as the sample-by-sample difference between the resampled SPICE and WDF data), and per-sample Newton iteration and backtrack counts. While $T_{1B}$ and $T_{1N}$ draw negligible grid current for all volume settings and input voltages studied $T_2$ and $T_3$'s grid currents reach appreciable fractions of the corresponding total cathode currents. Furthermore, the maximum values of these two grid currents are achieved with a 180° relative phase shift. This makes sense since the inputs to these two stages are 180° out of phase, the voltage amp stage involving $T_2$ being an inverting stage. The regions where $T_3$'s grid current reaches its maximum are the more heavily clipped positive output excursions. This asymmetric clipping is crucial to the generation of even order harmonics and emphasizes the importance of including the effects of grid currents in triode simulations if they are to capture this expected behavior.

The maximum error signal is approximately 30 mV for an output signal with a peak-to-peak voltage of approximately 165 V, representing an error of less than 0.2%. The SPICE results have been resampled onto the regular time grid of the WDF simulation in order to calculate the error signal. The Newton solver shows a remarkably low 3.03 average iterations and 0.08 backtracks per audio sample for $\alpha = 1.0$.

The WDF and SPICE simulation results are compared in the frequency domain for $\alpha = 1.0$ in Figure 10. Again, the SPICE results have been resampled onto the WDF simulation's time grid ($f_s = 176.4$ kHz) to enable spectral analysis and a Blackman window has been applied. Additionally, the SPICE data have been offset horizontally by 100 Hz to improve intelligibility, as other-

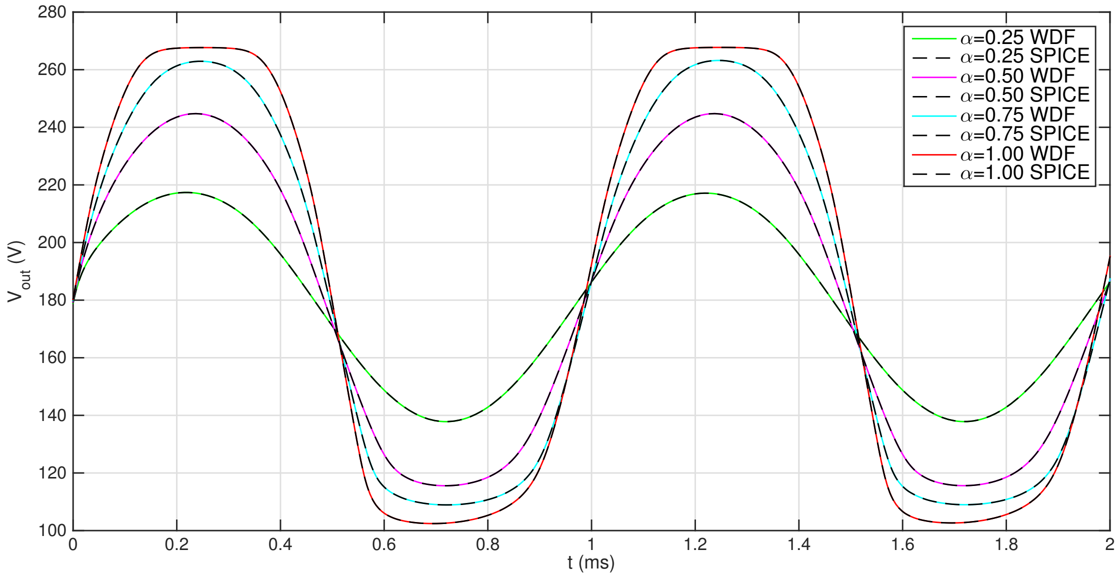


Figure 8: *WDF and SPICE simulation results for a* 1 kHz, 125 mV *peak-to-peak sinusoidal input.*

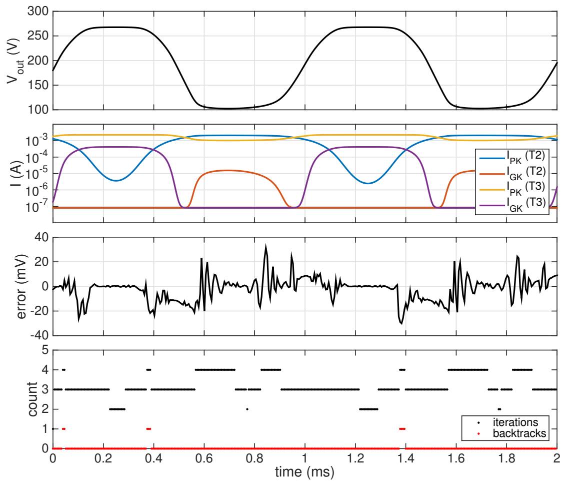


Figure 9: *WDF simulation results showing (top to bottom): output, triode $T_2$ and $T_3$ port currents, error (sample-by-sample difference between resampled SPICE and WDF results), and Newton iteration/backtrack count per audio sample (*1 kHz, 125 mV *peak-to-peak input,* $\alpha = 1.0$*).*

wise the peaks were more or less indistinguishable. The presence of strong even-order harmonics is characteristic of the asymmetric soft-clipping attributed to the inclusion of grid currents in the Dempwolf triode model. The relatively higher noise floor of the SPICE results is probably due to LTspice's tolerance settings (default values were used) and error introduced by resampling the variable-time-step SPICE data. No claims are made here as to the perceptual significance of this noise floor discrepancy, as psychoacoustic effects are not considered in this work.

QIFFT interpolation [26, 27] is applied to the spectral peaks revealing the first twenty harmonic peak frequencies to be identical to within less than 1 mHz. The interpolated dB peak magnitudes are listed in Table 2 and show remarkable agreement, differing by 0.1 dB or less up to the $17^{th}$ harmonic with a maximum deviation of 0.63 dB for the $18^{th}$ harmonic.

| Harmonic | SPICE | WDF | Harmonic | SPICE | WDF |
|---|---|---|---|---|---|
| *DC* | 143.31 | 143.31 | 11 | 73.61 | 73.54 |
| 1 | 130.72 | 130.72 | 12 | 79.08 | 79.09 |
| 2 | 114.76 | 114.76 | 13 | 70.99 | 70.99 |
| 3 | 113.57 | 113.57 | 14 | 73.52 | 73.55 |
| 4 | 104.53 | 104.52 | 15 | 67.74 | 67.70 |
| 5 | 91.24 | 91.23 | 16 | 64.81 | 64.81 |
| 6 | 86.96 | 86.94 | 17 | 64.32 | 64.22 |
| 7 | 89.42 | 89.42 | 18 | 53.80 | 53.17 |
| 8 | 81.37 | 81.37 | 19 | 57.29 | 57.55 |
| 9 | 80.28 | 80.28 | 20 | 55.93 | 56.21 |
| 10 | 73.41 | 73.46 | – | – | – |

Table 2: *SPICE and WDF frequency response interpolated peak values in dB (*1 kHz, 125 mV *peak-to-peak input,* $\alpha = 1.0$*).*

Finally, exponential sine sweeps [28] ranging from 20 Hz to 20 kHz over a 10 s time interval are used as inputs to the WDF simulation. Results for $\alpha = 0.25$ and $\alpha = 0.75$ are shown in the spectrograms of Figures 11 and 12 respectively. These results confirm that the model is well-behaved for input frequencies across the audible range and that the model's response features the expected increase in intensity of higher harmonics as volume is increased.

## 5. CONCLUSION AND FUTURE WORK

### 5.1. Future Work

As the current work models a single fixed jumper cable configuration, a future expanded preamplifier study will focus on including a fully general, real-time switchable jumper model. This will rely

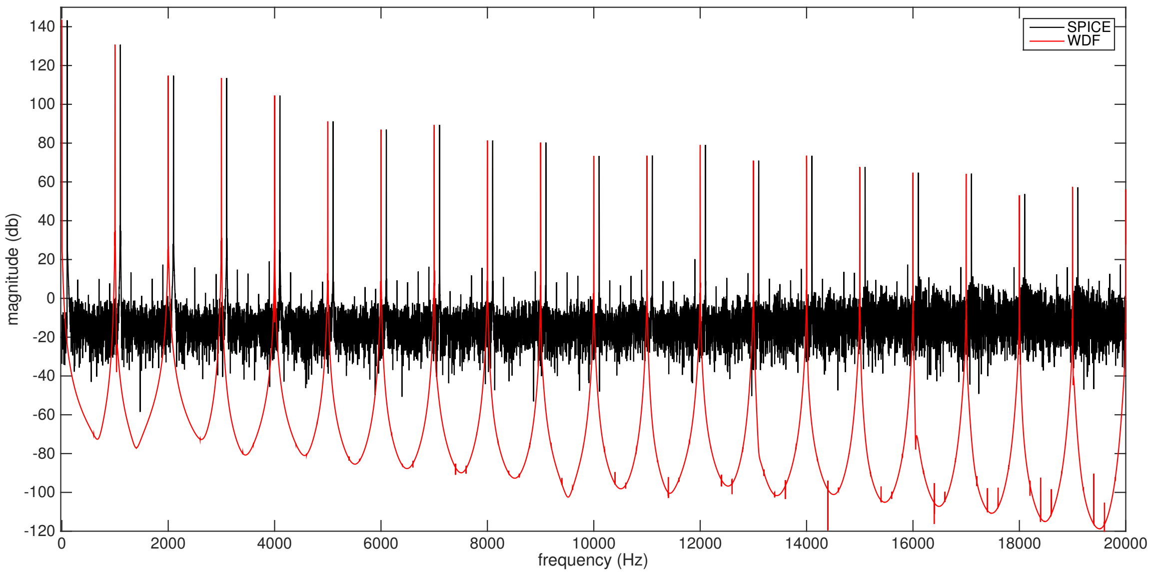


Figure 10: *WDF and SPICE frequency domain responses, SPICE offset by* 100 Hz *for clarity (*1 kHz, 125 mV *peak-to-peak input,* $\alpha = 1.0$*).*

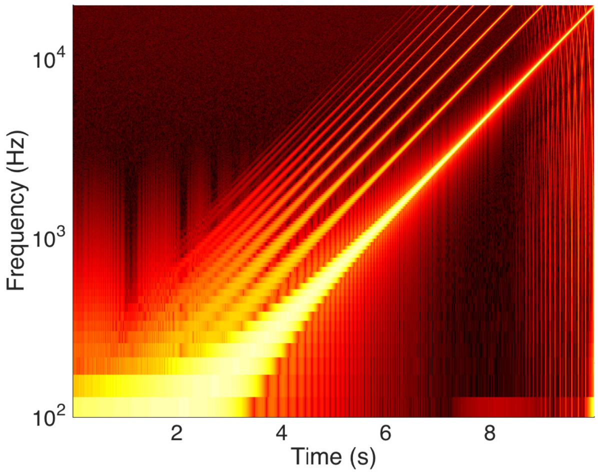


Figure 11: *Exponential sine sweep response spectrogram.* 125 mV *peak-to-peak input,* $\alpha = 0.25$.

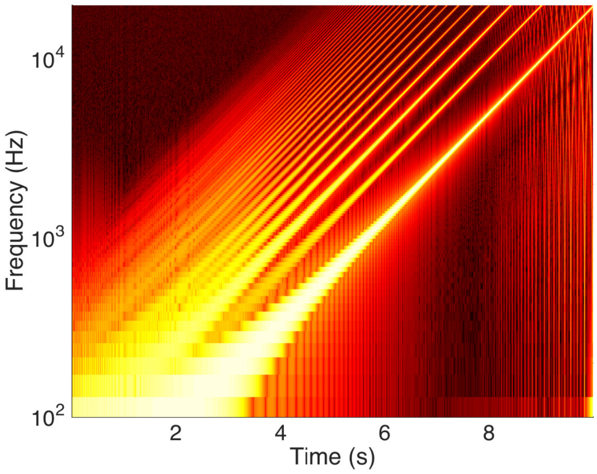


Figure 12: *Exponential sine sweep response spectrogram.* 125 mV *peak-to-peak input,* $\alpha = 0.75$.

on recent theoretical developments that enable WDFs to accommodate multiple non-adapted linear root elements [29]. The effects of stray pin capacitance will also be considered, most significantly the enhanced Miller equivalent capacitance [11] between plate and grid. It is our hope that Dempwolf model parameters for 12AY7 triodes can be obtained to facilitate comparison of the 5F6-A circuit's response to that of the JTM 45. Further triode models will also be evaluated and compared to the Dempwolf results presented here. To yield a complete, stand-alone preamplifier model the tone stack will also be incorporated into the WDF structure.

The current WDF simulation is in the process of being implemented and optimized in RT-WDF—a C++ real-time framework for WDF simulation described in [30]. Though the simulation is currently running slightly slower than real-time in an offline rendering utility, it is our hope and belief that further optimization will yield better-than-real-time performance.

Finally, it is worth noting that the most significant deviations of the JTM 45 design occur later in the amplifier's signal chain. For one thing, the Marshall utilizes significantly more negative feedback to drive the long-tail pair that feeds the push-pull power amp [1]. Also, while early JTM 45's utilized Radio Spares Deluxe [2] output transformers, the 5F6-A featured the Triad model 45249. Perhaps most significantly, the first Marshall cabinets made to accompany the JTM 45 were closed-back $4 \times 12$ designs loaded with Celestions G12 speakers whereas the Bassman 5F6-A was an open-backed $4 \times 10$ combo featuring Jensen P10Q's. Therefore in addition to continued refinement of the preamplifier model it is our aim to keep moving down the signal path, producing WDF models of as many of these elements as possible.

### 5.2. Conclusion

The WDF simulation results for the JTM 45 preamplifier show excellent agreement with SPICE "ground truth" results for a range of input signals and volume settings. In contrast to other WDF tube amplifier studies no ad-hoc assumptions are made, obviating the necessity for domain knowledge in analyzing the circuit and setting up the simulation. The only simplification is the use of a simple load resistance $R_L$ to represent the downstream circuit. When considered alongside a previous study of the Fender tone stack [6], the entire preamplifier circuit of Bassman-derived amplifiers has now been accurately modeled using WDFs. The use of Newton solver to calculate the nonlinear scattering at the root instead of tabulated methods leads to a much more compact memory footprint. It further allows the algorithm designer to trade simulation accuracy for computation time in a dynamic way by tuning the solver's tolerance parameter.

## 6. ACKNOWLEDGEMENTS

The author wishes to thank Jonathan Abel for enlightening conversations, his always unique perspective, and his generosity with baked goods.

## 7. REFERENCES

[1] Richard Kuehnel, *Circuit Analysis of a Legendary Tube Amplifier: The Fender Bassman 5F6-A*, Amp Books, Seattle, 2009.

[2] Michael Doyle, *The History of Marshall: The Illustrated Story of "The Sound of Rock"*, chapter The JTM 45 Series 1962–1966, pp. 17–22, Hal Leonard Corporation, Milwaukee, 1993.

[3] Jyri Pakarinen and David T. Yeh, "A review of digital techniques for modeling vacuum-tube guitar amplifiers," *Computer Music Journal*, vol. 33, no. 2, pp. 85–100, Summer 2009.

[4] Alfred Fettweis, "Wave digital filters: Theory and practice," *Proceedings of the IEEE*, vol. 74, no. 2, pp. 270–327, 1986.

[5] Giovanni De Sanctis and Augusto Sarti, "Virtual analog modeling in the wave-digital domain," *IEEE Transactions on Audio, Speech, and Language Processing*, vol. 18, no. 4, pp. 715–727, May 2010.

[6] Kurt J. Werner, Julius O. Smith III, and Jonathan S. Abel, "Wave digital filter adaptors for arbitrary topologies and multiport linear elements," in *18th International Conference on Digital Audio Effects (DAFx-15)*, Trondheim, Norway, November 30 – December 3 2015.

[7] Kurt J. Werner, Vaibhav Nangia, Julius O. Smith III, and Jonathan S. Abel, "Resolving wave digital filters with multiple/multiport nonlinearities," in *18th International Conference on Digital Audio Effects (DAFx-15)*, Trondheim, Norway, November 30 – December 3 2015.

[8] Kurt J. Werner, Vaibhav Nangia, Julius O. Smith III, and Jonathan S. Abel, "A general and explicit formulation for wave digital filters with multiple/multiport nonlinearities and complicated topologies," in *Proceedings of the IEEE Workshop on Applications of Signal Processing to Audio and Acoustics (WASPAA)*, New Paltz, NY, October 18–21 2015.

[9] David T. Yeh and Julius O. Smith III, "Tutorial on wave digital filters," Available: `https://ccrma.stanford.edu/~dtyeh/papers/wdftutorial.pdf`, Jan. 25 2008.

[10] David T. Yeh and Julius O. Smith III, "Discretization of the '59 Fender Bassman tone stack," in *Proc. Int. Conf. Digital Audio Effects (DAFx-06)*, Montréal, Canada, September 18–20 2006.

[11] John M. Miller, *Dependence of the input impedance of a three-electrode vacuum tube upon the load in the plate circuit*, vol. 15, pp. 367–385, Government Printing Office, Washington, 1919.

[12] Rob Robinette, "How Fender normal/bright/hi/low input jacks work," Available: `https://robrobinette.com/How_Fender_Input_Jacks_Work.htm`.

[13] Matti Karjalainen and Jyri Pakarinen, "Wave digital simulation of a vacuum-tube amplifier," in *IEEE International Conference on Acoustics, Speech and Signal Processing (ICASSP)*, Toulouse, France, May 14–19 2006, pp. 153–156.

[14] Peter Raffensperger, "Toward a wave digital filter model of the fairchild 670 limiter," in *15th International Conference on Digital Audio Effects (DAFx-12)*, York, UK, September 17–21 2012.

[15] Jyri Pakarinen and Matti Karjalainen, "Enhanced wave digital triode model for real-time tube amplifier emulation," *IEEE Transactions on Audio, Speech, and Language Processing*, vol. 18, no. 4, pp. 738–746, May 2010.

[16] Norman Koren, "Improved vacuum tube models for spice simulation," Available: `http://www.normankoren.com/Audio/Tubemodspice_article.html`.

[17] Jyri Pakarinen and Matti Karjalainen, "Wave digital modeling of the output chain of a vacuum-tube amplifier," in *12th International Conference on Digital Audio Effects (DAFx-09)*, Como, Italy, September 1–4 2009.

[18] Stefano D'Angelo, Jyri Pakarinen, and Vesa Välimäki, "New family of wave-digital triode models," *IEEE Transactions on Audio, Speech, and Language Processing*, vol. 21, no. 2, pp. 313–321, February 2013.

[19] Gian-Carlo Cardarilli, Marco Re, and Leonardo Di Carlo, "Improved large-signal model for vacuum triodes," in *International Symposium on Circuits and Systems (ICSCAS)*, Taipei, Taiwan, May 24–27 2009.

[20] Chung-Wen Ho, Albert Ruelhi, and Pierce Brennan, "The modified nodal approach to network analysis," *IEEE Transactions on Circuits and Systems*, vol. 22, no. 6, pp. 504–509, 1975.

[21] Dietrich Fränken, Jörg Ochs, and Karlheinz Ochs, "Generation of wave digital structures for networks containing multiport elements," *IEEE Transactions on Circuits and Systems–I: Regular Papers*, vol. 52, no. 3, pp. 586–596, 2005.

[22] W. Ross Dunkel, "Bassman/JTM 45 preamp WDF study supplemental materials for DAFx 2016," Available: `https://ccrma.stanford.edu/~chigi22/bassmanDAFx16/supplementalMaterials.html`.

[23] Michael Jørgen Olsen, Kurt James Werner, and Julius O. Smith III, "Resolving grouped nonlinearities in wave digital filters using iterative techniques," in *19th International Conference on Digital Audio Effects (DAFx-16)*, Brno, Czech Republic, September 5–9 2016.

[24] Kristjan Dempwolf and Udo Zölzer, "A physically-motivated triode model for circuit simulations," in *14th International Conference on Digital Audio Effects (DAFx-11)*, Paris, France, September 19–23 2011.

[25] Thomas Jungmann, "Theoretical and practical studies on the behavior of electric guitar pickups," M.S. thesis, Department of Electrical Engineering, Acoustics Laboratory, Helsinki University of Technology, Espoo, Finland, 1994.

[26] Julius O. Smith III and Xavier Serra, "Parshl: An analysis/synthesis program for non-harmonic sounds based on a sinusoidal representation," Available: `https://ccrma.stanford.edu/~jos/parshl/`.

[27] Mototsugu Abe and Julius O. Smith III, "Design criteria for simple sinusoidal parameter estimation based on quadratic interpolation of fft magnitude peaks," in *117th Convention of the Audio Engineering Society*, San Francisco, CA, October 28–31 2004.

[28] Angelo Farina, "Simultaneous measurement of impulse response and distortion with a swept-sine technique," in *108th Convention of the Audio Engineering Society*, Paris, France, February 19–22 2000.

[29] Kurt J. Werner and W. Ross Dunkel, "A computational model of the hammond organ vibrato/chorus using wave digital filters," in *19th International Conference on Digital Audio Effects (DAFx-16)*, Brno, Czech Republic, September 5–9 2016.

[30] Maximilian Rest, W. Ross Dunkel, Kurt J. Werner, and Julius O. Smith III, "RT-WDF—a modular wave digital filter library with support for arbitrary topologies and multiple nonlinearities," in *19th International Conference on Digital Audio Effects (DAFx-16)*, Brno, Czech Republic, September 5–9 2016.